Dynamics of phase separation of a simple fluid mixture: Comparison between molecular dynamics and numerical integration of the phenomenological equation

H. Furukawa
Faculty of Education, Yamaguchi University, Yamaguchi 753, Japan
(Received 26 July 1996; revised manuscript received 20 September 1996)

The dynamics of phase separation of fluid mixture is discussed. Numerical simulations in two dimensions are done both by means of the molecular dynamics at constant temperature and by the numerical integration of a phenomenological kinetic equation. Using a simplified interparticle potential, we find that final results in the molecular dynamics are seriously affected by numerical errors. The growth exponent of phase-separating domains varies from 1/3 to 2/3 due to the numerical errors for a low-viscosity fluid mixture with a critical composition. The exponent 2/3 is observed in the case where the numerical error is ineffective. On the other hand, the numerical error in the numerical integration of the phenomenological equation is not serious, and we obtain the growth exponent 2/3, as has been observed by many other similar numerical analyses. We also discuss possibilities of new growth exponents that are simultaneously associated with the inertia and the dissipation. [S1063-651X(97)03601-5]

PACS number(s): 02.70.−c, 64.70.Ja, 64.75.+g, 05.70.Ln

I. INTRODUCTION

Over more than two decades much attention has been paid to the dynamics of phase separation from the viewpoints of basic nonequilibrium statistical physics and material science [1–7]. The phase separation is treated as an irreversible process that does not reach a thermal equilibrium state. Among several kinds of systems the fluid is peculiar because of its fluidity. The fluidity is often characterized by inertia. The effect of the inertia on the phase separation of fluid has been discussed in terms of theoretical [8] and numerical simulations [9–20] as a direct observation of phase separation and also theoretically as the phase separation with shear [21]. One of the purposes of investigating the fluid system is to know how the inertia of the fluid affects the phase-separation process, because the inertia has a purely mechanical origin, is associated with the time-reversal symmetry of dynamics, and is inevitable in any large-scale motion. A similar problem arises in hydrodynamic turbulence. It is predicted that the characteristic length scale R varies as $t^{2/3}$ as a function of time t in two- and three-dimensional low-viscosity fluids [8] if the binary system is phase separating with interconnected domain morphology, which appears for critical compositions (in three dimensions near the critical temperature the growth law is linear in time t, i.e., $R \propto t$, if the length scale is not large [22]). However, this growth law is still controversial from the viewpoint of numerical simulations. Methods of numerical simulations can be classified into two categories: One is simulation by phenomenological models [9–11,17–20], where thermodynamic properties of the system are already taken into account, and the other is simulation by molecular dynamics [12–16], where thermodynamic properties have to be attained simultaneously. Methods by phenomenological models give the growth exponent 2/3, whereas molecular dynamics often gives different results. Several problems or questions must be examined to clarify this discrepancy between phenomenological and molecular-dynamical simulations. The first is that simulations are done mainly in two dimensions. It may be plausible that in two dimensions the phenomenological equation itself is invalid, i.e., the validity of the two-dimensional hydrodynamic equation may be questionable. Therefore, starting from the mechanical equation, any behavior expected by the hydrodynamic equation cannot be observed. The second concern is about the system size. Are system sizes for previous molecular dynamics large enough to attain the collective motion of the fluid and therefore to attain suitable fluid phase separations? The third question is whether there is any fundamental difficulty in achieving thermodynamic properties by numerical molecular dynamics. This is because molecular dynamics is seriously affected by the chaotic behavior of the many-particle system [23]. In this paper we focus our attention on the second and third problems. Because our aim is not to obtain rigorous quantitative results for the realistic molecular system but to know qualitative properties of the phase separation of the many-particle system, we employ a simpler interparticle potential that saves computational time, and makes the system size effectively large. Then we find that the molecular dynamics is affected by numerical errors in a serious way. We show also that a careful molecular dynamics gives the same growth exponent 2/3 as phenomenological treatment. At this moment we consider that the first problem is not serious to the phase separation.

In this paper we discuss how the molecular-dynamical treatment is qualitatively affected by the chaotic behavior of particle system and how we obtain a correct result from molecular dynamics. We examine also the simulation based on phenomenological equations, but we do not meet the same problem as for the particle system.

In the next section the essence of the growth exponent is given with the aid of the dimensional analysis. A new exponent is predicted; however, this exponent is not yet observed. In Sec. III we present several numerical results by molecular dynamics. In Sec. IV we discuss how the chaotic behavior of the particle system influences the molecular dynamics. We also present some numerical results using a phenomenologi-

cal equation in Sec. V. In Sec. VI we present concluding remarks.

II. TEMPORAL EVOLUTION OF THE PHASE SEPARATION

Inside the coexistence curve the thermodynamic instability causes a phase separation. In principle, the temporal evolution of the system from a homogeneous to a phase-separated inhomogeneous state can be found by solving the equation of motion. But this is generally not tractable. In the limit of the large characteristic length scale, the microscopic length scale can be reduced to zero. Once the microscopic scale is reduced to zero, the explicit value of macroscopic scale is often not important: The system becomes scale invariant. In this case one may extract a universal aspect of the dynamical behavior without solving the equation of motion. There are some microscopic physical quantities that characterize the dynamics of system, such as particle mass, particle number density, and surface tension. These quantities are closely related to the macroscopic behavior of the system. The macroscopic length scale R and time scale t are related to these microscopic quantities. Let $[m]$, $[l]$, and $[t]$ be dimensions of mass, length, and time, respectively. The surface tension σ, the kinetic viscosity ν, and the mass density ρ are the characteristic physical quantities in the case where a relevant driving force is the surface tension. Dimensions of these quantities are, respectively,

$$[\sigma]=[m][l]^{3-d}[t]^{-2}, \quad [\nu]=[l]^2[t]^{-1}, \quad [\rho]=[m][l]^{-d}. \tag{1}$$

Eliminating $[m]$ from the first and the last relations, we obtain

$$[l]=\left(\frac{\sigma}{\rho}\right)^{1/3}[t]^{2/3}. \tag{2}$$

The second relation of Eqs. (1) is rewritten as

$$[l]=(\nu[t])^{1/2}. \tag{3}$$

Combining the above two relations, we can make the following type of relation:

$$[l]/[t]^a=A. \tag{4}$$

Here a and A are constants independent of the length and the time scales and hence this can be determined independently of the length scale. This means that a and A can be determined microscopically, but dimensions $[l]$ and $[t]$ are applicable to the corresponding macroscopic quantities. This is the essence of the growth process at phase separation. The macroscopic length scale R varies as $R\propto t^a$. The quantity a is called the growth exponent. There may be number of sets of a and A. Let us replace $[l]$ and $[t]$ by the macroscopic length scale R and macroscopic time t. We find that simple combinations of σ and ν give important growth exponents. That is, σ itself gives $R\sim(\sigma/\rho)^{1/3}t^{2/3}$, which is the surface tension driven and inertia controlled growth law [8]. By solving Eqs. (2) and (3) for σ and ν we find that σ/ν gives $R\sim\sigma t/\rho\nu$, which is the surface tension driven and dissipation controlled growth law [22]. In the same way $\sigma\nu$ gives $R\sim(\sigma\nu/\rho)^{1/5}t^{3/5}$. For a detailed discussion of this growth law, see Appendix A. This is the growth law in the case where clusters or domains are redestroyed by the kinetic energy released with cluster coarsening. This growth law would hardly be observed. More generally, by multiplying Eqs. (2) and (3) by weight factors x and $1-x$, we have

$$R=\sigma^{x/3}\rho^{-x/3}\nu^{(1-x)/2}t^{(x+3)/6}. \tag{5}$$

If we set $x=1$ then the above relation does not contain the kinetic viscosity ν and the relation gives $R\propto t^{2/3}$. If we set $x=3$ we obtain $R\propto t$. If we choose $x=3/5$ we find $R\propto t^{3/5}$. There are many other possible growth laws, but the origins of such growth laws are not clear.

For isolated clusters in fluid the surface tension does not effect the phase separation. In such a case the thermal fluctuation is a driving force. We have, for the thermal energy k_BT,

$$[k_BT]=[m][l]^2[t]^{-2}. \tag{6}$$

From this and the third relation of Eqs. (1) we eliminate the mass $[m]$,

$$[l]=\left(\frac{k_BT}{\rho}\right)^{1/(d+2)}[t]^{2/(d+2)}. \tag{7}$$

Combining the above relation with Eq. (3) we have

$$R=\left(\frac{k_BT}{\rho}\right)^{x/(d+2)}\nu^{(1-x)/2}t^{1/2[1-(d-2)x/(d+2)]}. \tag{8}$$

Also in this case it will become apparent that the following three values of x are relevant using the simplest combination of k_BT and ν. For $x=1$ the growth law does not depend on the kinetic viscosity ν and gives $R\propto t^{2/(d+2)}$, which is applied to clusters floating in vapor [8]. Choosing $x=(d+2)/d$ we have $R^d=k_BT\eta^{-1}t$, which is the cluster coagulation by Brownian motion [24]. The growth law in the case of cluster reseparation is given by choosing $x=(d+2)/(d+4)$ as $R\sim(\nu k_BT/\rho)^{1/(d+4)}t^{3/(d+4)}$. Notice that in two dimensions the growth law exponent is independent of x and is given as $R\propto t^{1/2}$. All kinds of processes driven by the thermal fluctuation have the same growth law exponent 1/2 in two dimensions.

The above dimensional analysis can be extended. Let $R=f_s(t,x)$ and $R=f_t(t,x)$ be the growth laws by the surface tension and thermal fluctuation. Then a combined growth law $R=f_s(t,x)^yf_t(t,x')^{1-y}$ is also a possible growth law.

III. NUMERICAL ANALYSIS OF MOLECULAR DYNAMICS

We have performed a numerical analysis of the molecular dynamics of a fluid mixture. The model we use in this paper is described by a temporally discretized Newton equation. For a single-particle system the equation is given by

$$\frac{\mathbf{r}(t+\Delta t)+\mathbf{r}(t-\Delta t)-2\mathbf{r}(t)}{\Delta t^2}=\mathbf{F}(t), \tag{9}$$

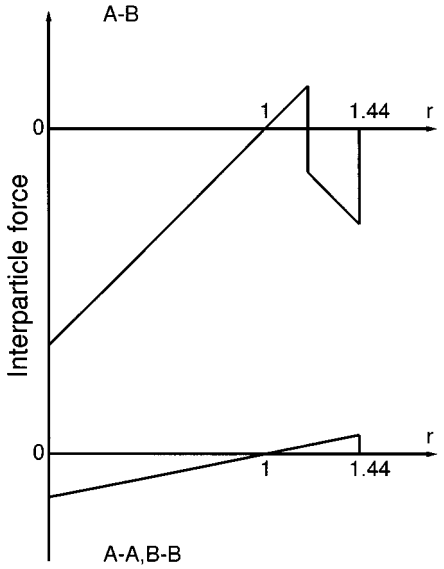

FIG. 1. Interparticle forces: upper, force between unlike particles; lower, force between like particles.

where $\mathbf{r}(t)$ and $\mathbf{F}(t)$ are the position and force at time t. The particle mass is set to unity. Δt is a discrete time interval. The mass of particle is set to 1. Equation (9) is the Veret algorithm [25] to simulate Newton's equation and it reduces to Newton's equation of motion in the limit $\Delta t \to 0$. The above equation of motion is symmetric with respect to the time reversal ($\Delta t \to -\Delta t$). This time-reversal symmetric equation can be transformed into a set of two different equations

$$\mathbf{r}(t+\Delta t)=\mathbf{r}(t)+\mathbf{v}(t)\Delta t, \tag{10}$$

$$\mathbf{v}(t+\Delta t)=\mathbf{v}(t)+\mathbf{F}(t+\Delta t)\Delta t, \tag{11}$$

where $\mathbf{v}$ is the velocity.

Numerical analyses for the many-particle system have been done in the following way. Initially A and B particles are randomly distributed on the square lattice sites with unit lattice spacing. The initial velocities of the particles are set randomly. The interparticle force we use here is as follows. Let A and B denote two species. We assume that a particle is acted upon by surrounding particles by the force (Fig. 1)

$$\mathbf{F}_{A,A}(\mathbf{r})=\mathbf{F}_{B,B}(\mathbf{r})=\begin{cases}\dfrac{\mathbf{r}}{r}(r-1) & \text{for } r<1.44\\ \mathbf{0} & \text{for } r>1.44,\end{cases} \tag{12}$$

$$\mathbf{F}_{A,B}(\mathbf{r})=\begin{cases}5\dfrac{\mathbf{r}}{r}(r-1) & \text{for } r<1.2\\ -5\dfrac{\mathbf{r}}{r}(r-1) & \text{for } 1.2\leqslant r\leqslant 1.44\\ \mathbf{0} & \text{for } r>1.44.\end{cases} \tag{13}$$

Here $\mathbf{F}_{\alpha,\beta}$ indicates forces between α and β particles. This is a truncated harmonic potential, with an extra repulsion between unlike particles. We also tried the Lennard-Jones-type potential, but we found that the numerical error is larger for such a steep potential and therefore much computational time is needed to obtain a reliable result. Otherwise, we must use a smaller system and we get a less reliable result. Because we are interested in the macroscopic behavior of the phase separation, such a microscopic structure of the interparticle force is not essential. Later we shall discuss why the molecular dynamics is not tractable to get reliable numerical results. This situation does not depend on explicit forms of the interparticle potential. Our interparticle potential is amplified between unlike particles. Then the domain interface becomes sharp and the system size is effectively large. The periodic boundary condition is used. We tried several values of Δt from $\frac{1}{2}$ to $\frac{1}{150}$. The simulations are done up to time 20×60. In each time interval 60 we obtain numerical data. We define the temperature by

$$T=\frac{1}{2k_B}\langle v_x^2+v_y^2\rangle. \tag{14}$$

We tried several values of temperature $k_BT=0.05^2$–0.9^2. The length scale $R(t)$ is defined by means of the structure function $S_k(t)$:

$$S_k(t)=\sum_{i>j} p_i p_j \exp i\mathbf{k}\cdot(\mathbf{r}_i-\mathbf{r}_j), \tag{15}$$

$$1/R(t)=\left(\frac{\int k^M S_k(t)\,dk}{\int S_k(t)\,dk}\right)^{1/M}. \tag{16}$$

Here $\mathbf{k}$ is the wave number vector and i and j indicate the ith and jth particles. $p=1$ for A particles and $p=-1$ for B particles. In practice, we calculate $S_k(t)$ by coarse graining the space into cells and using a fast Fourier transform. For the integration over k we cut off wave numbers larger than $6k_m$, where k_m is the peak position of the structure function, because the structure function at large wave numbers strongly reflects the effect of individual particles. We tried several values of M.

The number of particles is 256^2. The composition is 0.5, i.e., the number of A particles and B particles are the same. In most cases we used a discrete time $\Delta t=\frac{1}{60}$, except in the case where we examine the effect of Δt on the growth exponent a by the molecular dynamics. Most simulations are done under constant temperature. We used the simplest method to set a constant temperature. Namely, instead of Eq. (11) we use

$$\mathbf{v}(t+\Delta t)=\sqrt{\frac{T_0}{T(t)}}[\mathbf{v}(t)+\mathbf{F}(t+\Delta t)\Delta t], \tag{17}$$

where T is the temperature defined by Eq. (14) and T_0 is a constant. Using this equation the temperature of the system is kept at T_0. It should be noted that this procedure introduces a friction term into the difference equation. This friction term is not effective if the numerical integration is exact and the length scale R is large enough, because the change in the temperature is very small in such a case. However, as we shall show later, the increase in the temperature is very large

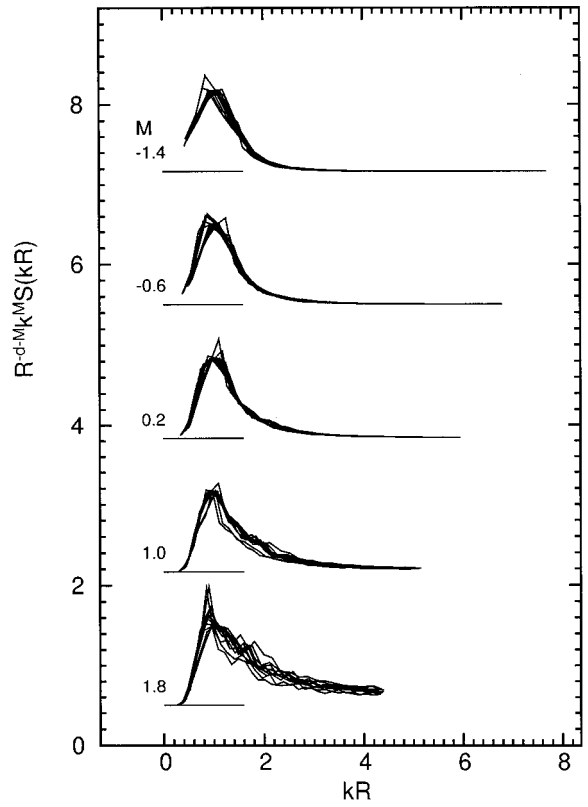

FIG. 2. Scaling plot of the structure function by molecular dynamics. $R^{-2-M}k^M S_k(t)$ is plotted as a function of kR for several values of M, which are shown in the figure.

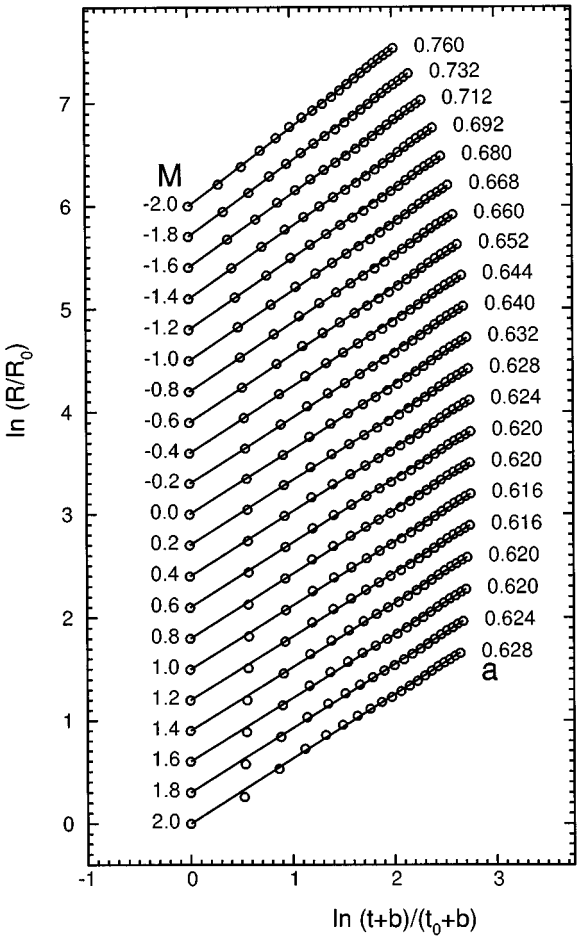

FIG. 3. Temporal evolution of length scales by molecular dynamics, which are determined by the least-squares method, for $k_BT=0.2^2$. The parameter M and growth exponent a are shown on the left- and on the right-hand sides, respectively. $t_0=60$ and $R_0=R$ at $t=t_0$ and b is a suitably determined value by the least-squares method. The vertical axis does not represent a correct zero point.

if Δt and therefore numerical error are large. In such a case the method of constant temperature gives rise to unexpected results. This will be discussed in Sec. IV. We tried the simulation also under the constant energy. In this case the initial velocities of all particles are set to zero. The final temperature is then about $k_BT\approx 0.42^2$. Figure 2 shows $R^{-2-M}k^M S(kR(t))$, which is the general form of the scaling plot. Here the case of $\Delta t=0.01$ is displayed. In Fig. 3 we show length scales as functions of time for various values of M. Here the growth exponent a for each value of M is calculated by the least-squares method

$$\delta_a I=\delta_b I=0, \tag{18}$$

where

$$I=\sum_t \left(\ln\frac{R(t_0)}{R(t)}+a\,\ln\frac{t+b}{t_0+b}\right)^2. \tag{19}$$

The summation over t is taken as $t=t_0,2t_0,3t_0,\ldots,20t_0$, which are times when data are taken. In Fig. 4 we show the length scale R as a function of time t for several temperatures. The straight line indicates the slope $\frac{2}{3}$. In Fig. 5 we plot the growth exponent a determined by the least-squares method at several temperatures. Here a rectangle with a black square represents a set of three values of a for $M=-1,0,1$ at constant temperature. By $M=0$ we mean a small M (≈ 0). We used $\Delta t=\frac{1}{60}$. A rectangle with a black circle represents a set of three data by the simulation under constant energy. All data are averages of four different runs.

We find that the growth exponent a takes values near 2/3 in the temperature regions $k_BT\approx 0.15^2$–0.5^2. Above 0.5^2 the growth exponent a gradually decreases. This is because the critical temperature is approached. Then the correlation length becomes larger and the critical slowing down occurs. Then it becomes difficult to get the growth exponent properly within a small system and a short-time interval. The exponent a also decreases as the temperature decreases. This is the case where the system solidifies and domains becomes frozen. We consider that the observed exponent $a\approx 2/3$ is equivalent to that observed by phenomenological models as well as predicted theoretically. At this moment we cannot determine a correct critical temperature. Figure 4 may indicate that the critical temperature locates around $k_BT\approx 0.5$ $(\sqrt{k_BT}\approx 0.7)$. We also evaluated the Reynolds number. The Reynolds number is estimated as $\mathrm{Re}\sim Ru/\nu$ and the characteristic velocity is estimated as $u\sim \delta R/\delta t$, where δt is the time interval of data output. The kinetic viscosity is estimated as $\nu\sim\tau_0 v$, where $v=\sqrt{k_BT}$ is the instantaneous velocity of particle and r_0 is the interparticle spacing for particle collisions. We may set $r_0\leqslant 1$. Let the one-dimensional system size be L. Then

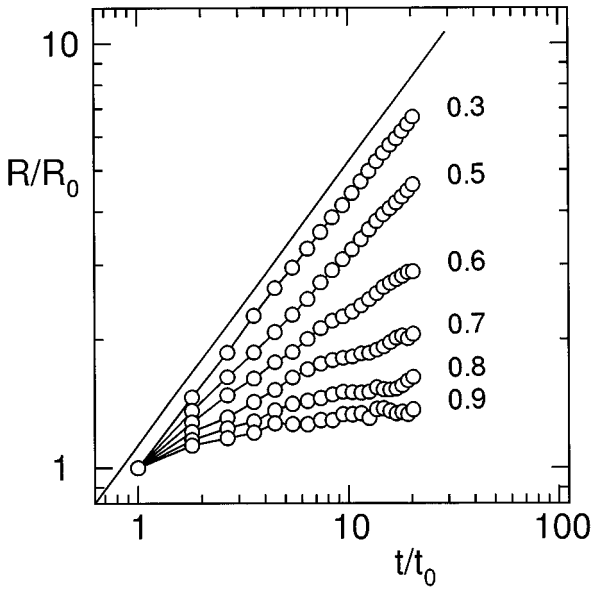

FIG. 4. Temporal evolution of length scale by molecular dynamics for various temperatures for $M \approx 0$. Here $t_0 = 60$ and $R_0 = R$ at $t = t_0$. The numbers on figure indicate $\sqrt{k_B T}$.

$Lk = 2\pi n$ $(n = 1,2,3, \ldots)$. Let n_m be the average of n, which gives the maximum of S_k. Then the length scale is also given by $R \sim L/n_m$. The approximate value of the Reynolds number estimated was more than 10 when the growth exponent is about 2/3.

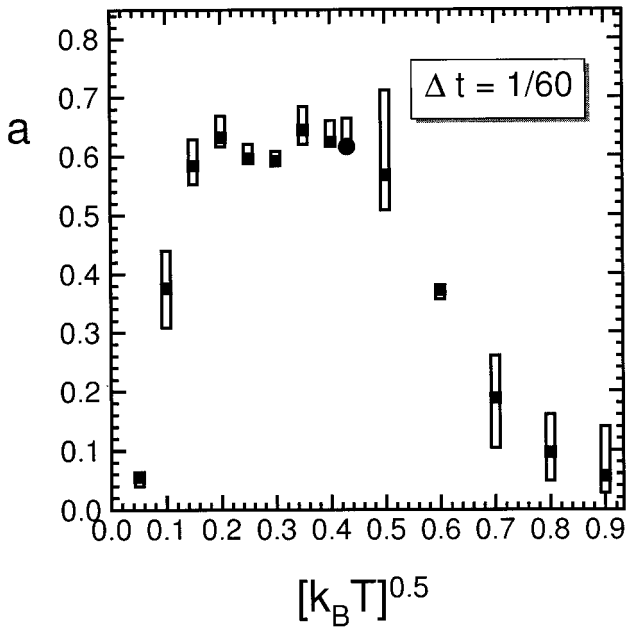

FIG. 5. Growth exponent a by molecular dynamics for various temperatures. The discrete time is chosen as $\Delta t = \frac{1}{60}$. A rectangle with a black square represents a set of exponents for $M = -1,0,1$ under constant temperature and a rectangle with a black circle is under constant energy. The temperature under constant energy is about $\sqrt{k_B T} \approx 0.42$.

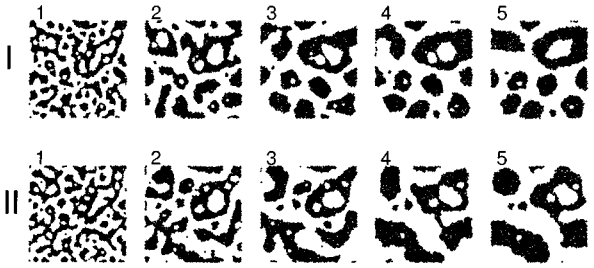

FIG. 6. Temporal evolution of phase-separating patterns by molecular dynamics at temperature $k_B T = 0.04$ $(\sqrt{k_B T} = 0.2)$. Two sequences labeled I and II start with slightly different initial conditions, namely, that the velocity of only one particle for sequence I is different from that for sequence II by an amount of only 10^{-10}. The number of particles is 64^2.

IV. NUMERICAL ERRORS FOR INTEGRATION OF THE EQUATION OF MOTION

When we integrate the equation of motion of the many-particle system we encounter difficulty that is seldom met with the phenomenological equation. The trajectory of dynamical motion in the many-particle system is intrinsically unstable. The motion of any particle is chaotic. This can be understood qualitatively as follows. Let us assume that the direction of motion of a particle deviates by a small angle $\Delta\theta$. Then at each collision with another particle this deviation is amplified because the collision is done on a positively curved surface. Then the deviation of a trajectory of a particle is increased exponentially as a function of time or collision number. This property is the source of the statistical nature of a system consisting of a large number of particles [26]. Therefore, the chaotic property of the system is necessary for the system to be described by a phenomenological equation such as the hydrodynamic equation. In the real system the transformation from the microscopic motion to the macroscopic motion is done perfectly. But by the numerical integration of the equation of motion the transformation cannot be done perfectly due to the chaotic property of the system. This is a technical problem that is not seen in real systems. This is the reason why it is difficult for molecular dynamics to obtain suitable results. Starting from the phenomenological equation, such difficulty hardly arises. The main motion we must deal with is the smoothing of domain interfaces. The interfacial motion does not increase the interfacial area but decreases it. Such a smoothing motion depends weakly on the initial condition and therefore is stable at least locally (this may also be the basis of the idea of cell dynamics [27]). This is the reason why the numerical analysis by the phenomenological equation is safer than molecular dynamics. We present here how numerical integrations of the molecular-dynamical equation depend on initial conditions. In Fig. 6 we show temporal evolutions of phase-separating patterns by molecular dynamics. Only a single species of particles is displayed. The temperature is $k_B T = 0.2^2$ and the number of particles is 64^2. The time interval between successive patterns in each sequence is 60. Two sequences I and II start from different initial conditions. The difference in the initial condition, however, is very small. That is, the initial velocity of only one particle in sequence I is different only by 10^{-10} from that of sequence II. A completely different morphology emerges between the two sequences.

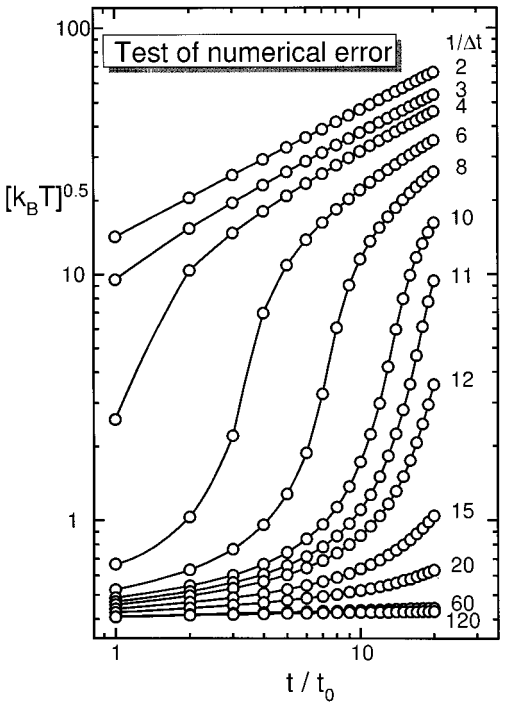

FIG. 7. Temperature as a function of time t for various values of Δt in the case where velocities are not rescaled by the molecular dynamics. This represents the effect of the numerical error to the temperature. The numbers shown on the right-hand side are values of $1/\Delta t$. Here $t_0=60$. Each set of data is taken from a single run.

In principle, molecular dynamics should give the same average behavior as the phenomenological method if the numerical integration is perfect. The chaotic property of the particle system is essentially needed to attain the thermodynamic property of the system. Therefore, one may consider that the numerical errors would simply be transformed into statistical properties and hence we may simply renormalize the thermodynamic quantities such as pressure, temperature, and internal energy. But our numerical analysis will show that this is not true. For the fluid dynamics the effect of the numerical error is serious. We explain this here. Our explanation is not rigorous, but only qualitative.

First let us consider the case where we do not rescale the velocity. If the numerical integration is exact, this is the case of the simulation under constant energy. But for large Δt the condition of constant energy is not satisfied. In Fig. 7 we show the increase in the temperature of the system as a function of time for various values of Δt. The simulation is done under the same conditions as in Sec. III. The initial temperature is set to about zero. For large Δt we find that the temperature increases linearly with time $T \propto t$. At least for two values of $\Delta t = \frac{1}{2}$ and $\frac{1}{3}$, we can find that T is proportional both to t and Δt, i.e., $T \propto t \Delta t$. For large Δt we observe that $k_B T \gg k_B T_c \approx 0.5$. Such a large increase in the temperature cannot be explained by the particle interaction. Therefore the increase in the temperature for large T is due to the numerical error. Let $\mathbf{W}$ be the error due to the discretization of the equation of motion (9). Then Eq. (9) is rewritten by a differential equation, by expanding $\mathbf{r}$, as

$$\frac{d\mathbf{v}(t)}{dt} = \mathbf{F}(t) + \mathbf{W}(t). \tag{20}$$

Since particles move in a chaotic way, the numerical error $\mathbf{W}(t)$ can be treated as a random variable. In fact, the behavior of T for large Δt can be explained by the fact that $\mathbf{W}$ is a random force. This is because, neglecting $\mathbf{F}$ in Eq. (20) due to $T \gg T_c$ and using a standard technique (for instance, see [2]), we obtain

$$\frac{d}{dt}\langle \mathbf{v}^2 \rangle = 2 \int_{-\infty}^{t} \langle \mathbf{W}(t) \cdot \mathbf{W}(t') \rangle \, dt' = 2Q, \tag{21}$$

where we have set

$$\langle \mathbf{W}(t) \cdot \mathbf{W}(t') \rangle = 2Q \delta(t - t'). \tag{22}$$

We may assume that Q is independent of time because an intrinsic chaotic motion of particles is the source of the randomness of $\mathbf{W}$. Since the temperature is given by Eq. (14) we find that the temperature increases linearly. For small $\Delta t \sim \frac{1}{60}$, T increases only slightly as a function of time t. In this case the effect of the numerical error on the temperature is considered to be small. The increase in the temperature is also due to domain growth by which the surface energy is released. Most of the potential energy is released in the initial stage of the phase separation and therefore the increase in the temperature is not effective in later stages of the phase separation. For the intermediate values of Δt the temperature becomes affected seriously by the numerical error as time proceeds. Notice that such an effect always occurs even for smaller value of Δt as time proceeds.

Now let us consider the case of a simulation under constant temperature. This case is equivalent to introducing an effective friction term. The frictional coefficient is common to all particles. This violates the local momentum conservation. Therefore, if the effect of the numerical error cannot be neglected, the macroscopic equation is not like the Navier-Stokes equation but like the Langevin equation in the light of the standard statistical mechanics. Let us assume that the equation for the macroscopic motion contains a friction term $-\gamma_{\text{eff}}\mathbf{v}$, which is not like that of the Navier-Stokes equation but of the Langevin equation. Here $\mathbf{v}$ means the velocity of the macroscopic motion. The friction term $-\gamma_{\text{eff}}\mathbf{v}$ is related to the random force $\mathbf{W}(t)$ by the usual fluctuation-dissipation theorem

$$\gamma_{\text{eff}} = \frac{Q}{\langle \mathbf{v}^2 \rangle}. \tag{23}$$

The characteristic velocity $u \equiv R/t$ should obey a dimensional equation

$$\frac{u}{t} \approx -\gamma_{\text{eff}} u + \frac{\sigma}{\rho R^2}, \tag{24}$$

where the second term on the right-hand side is the driving force by the surface tension. This is transformed into

$$R^{-1} \approx \left(\frac{\rho}{\sigma}\right)^{1/3} (t^{-2} + \gamma_{\text{eff}} t^{-1})^{1/3}. \tag{25}$$

Then the effective growth exponent a_{eff} is given as

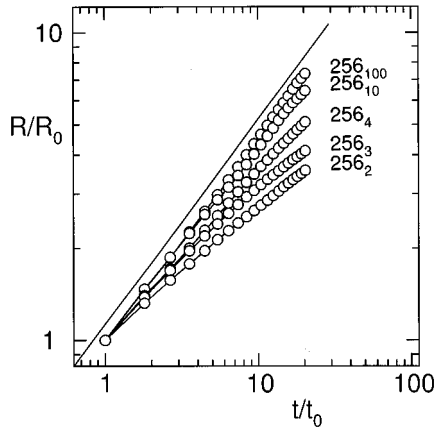

FIG. 8. Temporal evolution of the length scale by molecular dynamics for various discrete times Δt at temperature $k_BT=0.2^2$. Numbers in the figure indicate sets of system size and the value of inverse discrete time $1/\Delta t$. Here $t_0=60$ and $R_0=R$ at $t=t_0$.

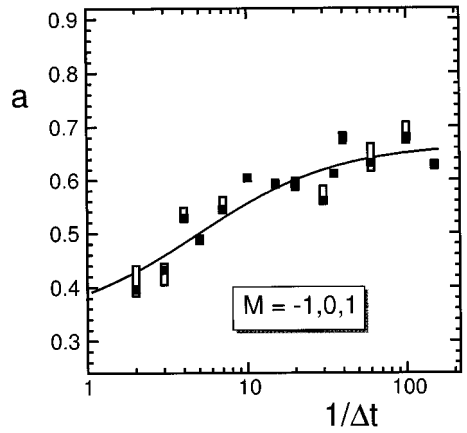

FIG. 9. Growth exponent a as a function of $1/\Delta t$ by molecular dynamics at temperature $k_BT=0.2^2$. One rectangle with black square indicates a set of three exponents for $M=-1,0,1$. The curve indicates Eq. (26), where we have set $\gamma_{\rm eff}t\sim Zt\Delta t\sim 5\Delta t$.

$$a_{\rm eff}\equiv\frac{d\ \ln R}{d\ \ln t}\approx\frac{(\frac{2}{3}+\frac{1}{3}\gamma_{\rm eff}t)}{(1+\gamma_{\rm eff}t)}. \tag{26}$$

Since $\gamma_{\rm eff}$ is larger for larger Δt, $a_{\rm eff}$ crosses over from 2/3 to 1/3 as t and/or Δt becomes larger. In Fig. 8 length scales obtained by the molecular dynamics are shown as functions of time for some values of $1/\Delta t$. The temperature is $k_BT=0.2^2$ and the number of particles is 256^2. The simulation is done up to time 20×60. In Fig. 9 we show the corresponding growth exponents determined by the least-squares method at temperature $k_BT=0.2^2$ for several values of $1/\Delta t$. Each rectangle with a black square represents a set of three exponents for $M=-1,0,1$. The curve on the figure indicates Eq. (26). Here we have assumed that $\gamma_{\rm eff}\sim Z\Delta t$, where Z is a constant. Further we neglected the t dependence in Eq. (26) and we have set $t\gamma_{\rm eff}\sim Zt\Delta t\sim 5\Delta t$. In the last equality of this equation we have replaced Zt simply by 5 because we are interested in the Δt dependence of $a_{\rm eff}$. At this moment we cannot analytically determine the dependence of the $\gamma_{\rm eff}$ on Δt. The prediction (26) is qualitatively satisfied. It can be also found that $\Delta t=\frac{1}{60}$, which is used in Sec. III, is not small enough to obtain the suitable growth exponent 2/3.

V. NUMERICAL ANALYSIS OF INTEGRATION OF PHENOMENOLOGICAL EQUATIONS

Here we present results given by the numerical integration of phenomenological kinetic equations. Phenomenological kinetic equations of fluid mixture have been developed by many authors (see, for instance, [28]). Let $n_A(\mathbf{r})$ and $n_B(\mathbf{r})$ be particle densities of A and B species and $\mathbf{v}(\mathbf{r})$ be the velocity field. Then we introduce another set of variables

$$\psi\equiv n_A-n_B, \tag{27}$$

$$n\equiv n_A+n_B. \tag{28}$$

We assume that the free energy is given by

$$F=\int\left(\frac{\rho}{2}v^2+\frac{1}{2}\chi^{-1}(n-n_0)^2+\frac{g}{2}|\nabla\psi(\mathbf{r})|^2+\frac{a'}{2}\psi^2+\frac{b'}{4}\psi^4\right)d\mathbf{r}. \tag{29}$$

Here ρ is the mass density of the fluid and is given as $\rho=nm$, where m is the mass of a molecule. Coefficients a', b', and m are set $-a'=b'=m=1$ and we also assume $\chi^{-1}\gg 1$ as an incompressible condition. Setting $a'=-1$, the free energy takes minima at $\psi=\pm 1$. In this case the two-phase state is stable. The quantities ψ and n must satisfy the continuity equations and therefore we assume

$$\frac{dn}{dt}=-\nabla\cdot\mathbf{j}_n, \tag{30}$$

$$\frac{d\psi}{dt}=-\nabla\cdot\mathbf{j}_\psi, \tag{31}$$

where the $\mathbf{j}$'s are currents

$$\mathbf{j}_n=n\mathbf{v}-L_n\nabla\mu_n^*,\quad \mu_n^*\equiv\frac{\delta F}{\delta n}, \tag{32}$$

$$\mathbf{j}_\psi=\psi\mathbf{v}-L_\psi\nabla\mu_\psi,\quad \mu_\psi\equiv\frac{\delta F}{\delta\psi}, \tag{33}$$

and the second term in each current represents the diffusion. μ_n^* is the chemical potential in a dynamical sense and contains the velocity field $\mathbf{v}$. Usually in many phenomenological theories the second term of $\mathbf{j}_n$ is neglected. But this does not mean that the role of μ_n^* can be neglected. We assume that the velocity field $\mathbf{v}$ obeys the Navier-Stokes equation

$$\rho\frac{d\mathbf{v}}{dt}=-\rho(\mathbf{v}\cdot\nabla)\mathbf{v}+\eta\nabla^2\mathbf{v}-\nabla P, \tag{34}$$

where η is the shear viscosity and is related to the kinetic viscosity ν by the relation

$$\eta=\rho\nu. \tag{35}$$

P is the static pressure. We consider the case of constant temperature. Then we can show that the Navier-Stokes equation (34) can be transformed into (see Appendix B)

$$\rho \frac{d\mathbf{v}}{dt} = -\rho(\mathbf{v}\cdot\nabla)\mathbf{v} + \eta\nabla^2\mathbf{v} - n\nabla\mu_n - \psi\nabla\mu_\psi, \tag{36}$$

where

$$\mu_n \equiv \frac{\delta F^{(0)}}{\delta n} = \chi^{-1}(n - n_0), \tag{37}$$

$$\mu_\psi \equiv \frac{\delta F}{\delta \psi} = -g\nabla^2\psi - \psi + \psi^3. \tag{38}$$

Here $F^{(0)}$ is the free energy for $\mathbf{v}=\mathbf{0}$. In solids $\mathbf{v}=\mathbf{0}$ due to the infinite friction. This corresponds to letting $\nu\to\infty$. As a result, the equation of motion for ψ is of a closed form and reduces to the Cahn-Hilliard equation [29]. In fluids, under the condition $\chi^{-1}\gg 1$, Eq. (36) can be solved to give the well-known kinetic equation of ψ using the Oseen tensor [30] (see Appendix C).

The numerical analysis of the incompressible fluid can be done by solving Eqs. (30)–(33) and (36)–(38). Notice that Eq. (30) is a subsidiary equation for the incompressibility of fluid. This equation may be replaced by simpler one. We neglected the diffusion term in Eq. (30):

$$\frac{dn}{dt} = -\nabla\cdot n\mathbf{v}. \tag{39}$$

Furthermore, for the sake of computational efficiency, we used another form of the chemical potential functional

$$\mu_\psi = -K\nabla^2\psi - \frac{\tanh\psi}{\tanh 1} + \psi, \tag{40}$$

which is shallower than the original one (38). Here K is a constant. Equation (40) is based on the algorithm introduced by Oono and Puri [27]. We have neglected any random forces. The thermal fluctuation is included only in the initial condition.

The numerical method is a simple Euler method. The system is divided into 256×256 cells. The discrete time is chosen to be 0.1. Shorter ones are also tried, but the results are not changed. The spatial derivative is replaced by differences such as $A(x+1,y)-A(x,y)$ or $[A(x+1,y)-A(x-1,y)]/2$. Then we chose parameters as $L_\psi = L_n = 1/4$, $\chi^{-1}=10$, and $K=1/8$. Choosing such a χ, we find that $n=1$ within a width of the order $\pm 10^{-4}$.

In Fig. 10 we show temporal evolutions of phase-separating patterns by the above phenomenological equation. The time interval between successive patterns in each sequence is 64. The system size is 64^2. The viscosity is $\nu=0.01$. Initially ψ is randomly distributed between $-0.25\leqslant\psi\leqslant 0.25$ and the velocity field is set to zero, i.e., $\mathbf{v}=\mathbf{0}$. The difference between the two sequences I and II is that the initial value of ψ in one of the cells is shifted by the amount 0.1. The two sequences exhibit some differences from each other, but these differences are small compared to the differences in the case of molecular dynamics in Sec. IV.

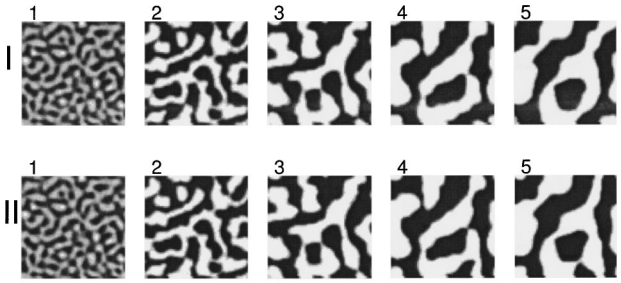

FIG. 10. Temporal evolutions of phase-separating patterns by the phenomenological equation. The kinetic viscosity $\nu=0.01$. The system is divided into 64×64 cells. Two sequences I and II start with different initial conditions, namely, that the order parameter of one of the cells for sequence I is different by the amount $\Delta\psi=0.1$ from that of sequence II.

Furthermore, the shift in the initial condition in the molecular-dynamical case is quite small compared to the present one. Therefore, we find that the two numerical methods, the molecular dynamics and the integration of the phenomenological equation, are quite different in tractability.

Now we present numerical results of the temporal evolution of the length scale in a larger system. Initially the velocity field $\mathbf{v}$ is set to zero and the order parameter is randomly distributed between $-0.75\leqslant\psi\leqslant 0.75$. The numerical integration is done up to time 20×128. In each time interval 128, we obtain numerical data. Figure 11 shows length scales as functions of time for a small value of the kinetic viscosity $\nu=0.01$. The straight lines are determined by the least-squares method (18). Data are averaged over ten different runs. The Reynolds number evaluated in this case is more than 1000. The growth exponent a is obtained for various values of M, which are shown in the figure.

In Sec. II we have shown that there are two similar growth exponents 2/3 and 3/5 associated with the inertia. In Appendix A we discuss fluctuations and energy dissipations in the process of the phase separation and we discuss these two growth laws in detail. We find that the coarsening process associated with the exponent 3/5 must accompany cluster reseparations. In our numerical simulations, however, cluster surfaces ramify, but clusters do not reseparate. In order for clusters to separate again, the energy must be concentrated in a narrow space. But such a concentration occurs with very small probability. We consider therefore, that the observed growth exponents indicate not 3/5 but 2/3.

VI. SUMMARY

The purpose of this paper was to examine the phase separation of a low-viscosity fluid mixture. We studied a two-dimensional fluid mixture both by the molecular dynamics with a simplified interparticle potential and by the numerical integration of the phenomenological equation. All studies are done for critical composition. We found that both types of simulations give the growth exponent $R\propto t^{2/3}$. Several phenomenological models have exhibited the same exponent $a=2/3$ [9–11,17–20]. We have shown that numerical errors in molecular dynamics seriously affect the phase-separation process. The growth exponent a decreases from 2/3 to 1/3 as numerical errors become larger. The source of such a reduc-

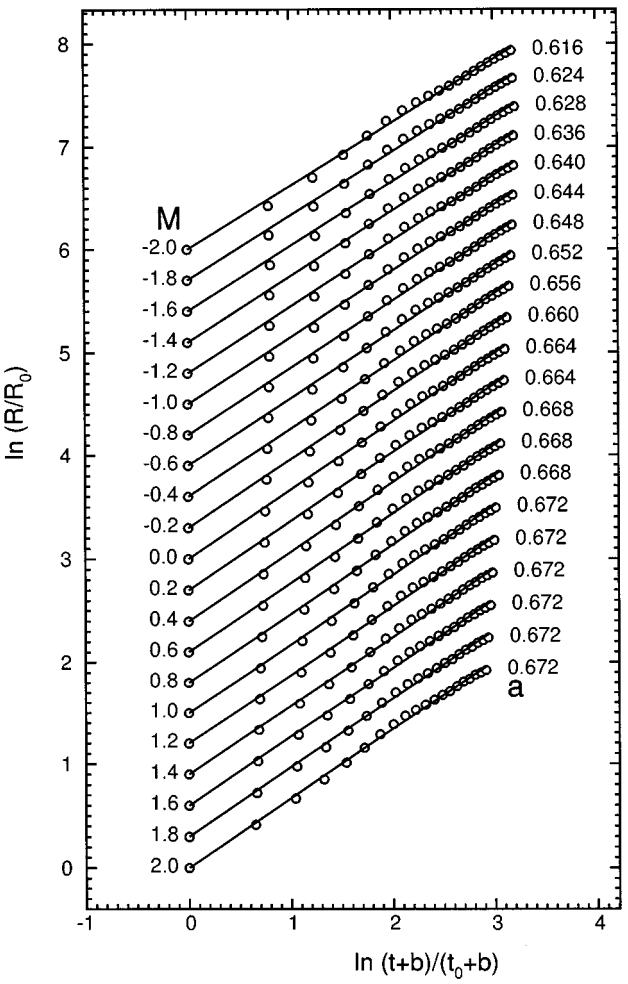

FIG. 11. Temporal evolution of length scales by the phenomenological equation, which are determined by the least-squares method. The parameter M and growth exponent a are shown on the left- and on the right-hand sides, respectively. $t_0=128$, $R_0=R$ at $t=t_0$, and b is a suitably determined value by the least-squares method. The vertical axis does not represent a correct zero point.

tion of the growth exponent is numerical errors arising from the chaotic property of the many-particle system. A previous molecular dynamics analysis gave a smaller growth exponent $a\leqslant 0.5$ [15]. In that molecular dynamics study a steeper Lennard-Jones-type interparticle potential was used. Generally the numerical error is larger for such a steeper potential. Therefore, it is worth examining the effect of the numerical error for such a steep potential. We also emphasize that the system size is responsible for obtaining a suitable growth exponent. In our simulation we observed a plateau of a as a function of temperature (see Fig. 5). This means that our system size is large enough.

We have used the simplest way of setting a constant temperature (17), which violates the local momentum conservation law. There may be a better way of setting a constant temperature. But remember that our primary purpose of the present paper was to examine the growth exponent a by the molecular dynamics. This purpose has been achieved.

In this paper we predicted another set of growth exponents $a=3/5$ and $6/(d+4)$, where the inertia and the energy dissipation are simultaneously associated with the domain growth. It is not obvious if such growth laws are really observed.

APPENDIX A: ENERGY DISSIPATION AND GROWTH LAWS ASSOCIATED WITH INERTIA

We examine here the energy dissipation in a fluid mixture in detail and then give a detailed discussion for the growth exponents 2/3 and 3/5 associated with inertia, based on the hydrodynamic equation. The energy dissipation sometimes is responsible for the growth exponent in solid systems [31]. For simplicity we write the equation for the velocity field $\mathbf{v}$ in the form

$$\rho\frac{d\mathbf{v}_\mathbf{k}}{dt}+\eta k^2\mathbf{v}_\mathbf{k}=\mathbf{F}_\mathbf{k}, \tag{A1}$$

where $\mathbf{k}$ is the wave number, $\eta=\nu\rho$ is the shear viscosity, and $\mathbf{F}$ is the force term. Equation (A1) is based on the Navier-Stokes equation. A general consideration of the equation of motion for the velocity field $\mathbf{v}$ is given in Appendix B. Equation (A1) is simplified as

$$\eta k^2\mathbf{v}_\mathbf{k}=\mathbf{F}_\mathbf{k} \quad \text{for} \quad \nu k^2 t \ \ (=\nu k^2 v/\dot{v})>1, \tag{A2}$$

$$\rho\frac{d\mathbf{v}_\mathbf{k}}{dt}=\mathbf{F}_\mathbf{k} \quad \text{for} \quad \nu k^2 t<1. \tag{A3}$$

From this the energy dissipation is separated into two parts

$$\dot{\epsilon}_D\equiv\sum_{\nu k^2 t>1}\eta k^2|v_\mathbf{k}|^2$$

$$=\sum_{\nu k^2 t>1}\frac{1}{\eta k^2}|\mathbf{F}_\mathbf{k}|^2\sim|\mathbf{F}_0|^2\eta^{-1}(k_l^{d-2}-k_c^{d-2}), \tag{A4}$$

$$\dot{\epsilon}_I\equiv\sum_{\nu k^2 t<1}\eta k^2|v_\mathbf{k}|^2\sim\sum_{\nu k^2 t<1}\eta\rho^{-2}k^2t^2|\mathbf{F}_0|^2, \tag{A5}$$

where we have set $\mathbf{F}_\mathbf{k}=\mathbf{F}_0$. Here k_c is the critical wave number determined by

$$\nu k_c^2 t=1. \tag{A6}$$

k_l is the upper limit of the integration and it is due to the freezing of the short wavelength due to the coarsening. For $k_l>k_c$, $\dot{\epsilon}_I\sim|\mathbf{F}_0|^2\eta\rho^{-2}t^2k_c^{d+2}\sim|\mathbf{F}_0|^2\eta^{-1}k_c^{d-2}$ and the total energy dissipation is given by

$$\dot{\epsilon}=\dot{\epsilon}_D+\dot{\epsilon}_I\sim|\mathbf{F}_0|^2\eta^{-1}k_l^{d-2} \quad \text{for} \quad k_l>k_c \tag{A7}$$

and

$$\dot{\epsilon}=\dot{\epsilon}_I\sim|\mathbf{F}_0|^2\eta\rho^{-2}t^2k_l^{d+2}\sim|\mathbf{F}_0|^2\eta^{-1}k_l^{d+2}/k_c^4 \quad \text{for} \quad k_l<k_c. \tag{A8}$$

The upper limit of the integration k_l is determined as follows. Let the average length scale be R. Then the total energy density is given by $\epsilon\sim\sigma/R$, where σ is the surface

tension. The energy dissipation is also given by $\epsilon/t \sim \sigma/Rt$ and therefore we find for $k_l > k_c$ that $|\mathbf{F}_0|^2 \eta^{-1} k_l^{d-2} \sim \sigma/Rt$ or $k_l^{d-2} \sim \eta\sigma/|\mathbf{F}_0|^2 Rt$. When the surface tension is effective, the force $\mathbf{F}$ in the real space is of the order $\epsilon/R \sim \sigma R^{-2}$. Therefore, in the Fourier space we have $|\mathbf{F}_0|^2 \sim \sigma^2 R^{d-4}$. Therefore, for $k_l > k_c$ we have

$$(k_l R)^{d-2} \sim \frac{\eta R}{\sigma t}. \tag{A9}$$

In the same way, for $k_l < k_c$ we have

$$(k_l R)^{d+2} \sim \frac{\eta}{\sigma t}(R k_c)^4 R. \tag{A10}$$

Let us consider the case where the inertia effects the domain growth. Then we examine the effect of the energy dissipation on the phase separation. First we consider the case where the domain growth is done independently of the energy dissipation. In this case the length scale R varies as discussed in Sec. II,

$$R \sim \left(\frac{\sigma}{\rho}\right)^{1/3} t^{2/3}. \tag{A11}$$

Now we consider the behavior of k_l. First let us consider the case of two dimensions. In the case $k_l > k_c$, using $(k_l R)^{d-2} \sim \eta R/\sigma t$, we obtain $k_l R \sim \exp \eta R/\sigma t \to 1$ $(R/t \to 0)$. Thus $k_l \sim 1/R \propto t^{-2/3}$. Since $k_c \propto t^{-1/2}$, the condition $k_l > k_c$ is violated in the long-time limit. On the other hand, for $k_l < k_c$ we have $k_l \propto t^{-7/12} \approx t^{-5.8}$. Then the condition

$$1/R < k_l < k_c \tag{A12}$$

is always fulfilled. The same also holds for three dimensions. For $k_l > k_c$ we have $k_l \propto 1/t$ and the condition $k_l > k_c$ is not satisfied in the long-time limit. On the other hand, for $k_l < k_c$ we have $k_l \propto t^{-3/5} = t^{-0.6}$ and the above condition is fulfilled.

Next we consider the case where the energy dissipation interferes with the domain growth. The wave number k_c is not observable. However, k_l is the cutoff of the velocity field, is observable, and gives another length scale. That is, the released surface energy at the scale R is dissipated at a smaller scale $1/k_l$: The kinetic energy remains in the fluid for this period. Due to such a remaining kinetic energy, it is possible that clusters may separate into pieces again. If such a reseparation occurs, then the limit of the wave number k_l should be the characteristic length scale R. Then we observe that $R \sim 1/k_l$ and $\epsilon \sim \sigma k_l$, and by setting $k_l R = 1$ in relation (A10) for $k_l < k_c$, we obtain

$$R \sim \left(\frac{\sigma\nu}{\rho}\right)^{1/5} t^{3/5}, \tag{A13}$$

which is given in Sec. II.

Generally, by setting $R \propto t^a$, the Reynolds number $\nu R^2/t$ increases if $a > 1/2$. The inertial term becomes effective for Reynolds number larger than 1. Three growth laws $R \propto t, t^{2/3}$, and $t^{3/5}$ give the same value of the length scale

$$R_c = \frac{\rho \nu^2}{\sigma} \tag{A14}$$

for Re$=1$ (the crossover point).

APPENDIX B: PHENOMENOLOGICAL DESCRIPTION OF FLUID MIXTURE

We derive here a suitable equation of motion for velocity field from the original Navier-Stokes equation (34). Since $n_A = (n+\psi)/2$ and $n_B = (n-\psi)/2$, we find that

$$\begin{aligned}\mu_n(\mathbf{r}) &\equiv \frac{\delta F^{(0)}}{\delta n} \\ &= \int \left[\frac{\delta n_A(\mathbf{r}')}{\delta n(\mathbf{r})} \frac{\delta F^{(0)}}{\delta n_A(\mathbf{r}')} + \frac{\delta n_B(\mathbf{r}')}{\delta n(\mathbf{r})} \frac{\delta F^{(0)}}{\delta n_B(\mathbf{r}')} \right] d\mathbf{r}' \\ &= \frac{\mu_A(\mathbf{r}) + \mu_B(\mathbf{r})}{2}\end{aligned} \tag{B1}$$

and

$$\begin{aligned}\mu_\psi(\mathbf{r}) &\equiv \frac{\delta F^{(0)}}{\delta \psi} \\ &= \int \left[\frac{\delta n_A(\mathbf{r}')}{\delta \psi(\mathbf{r})} \frac{\delta F^{(0)}}{\delta n_A(\mathbf{r}')} - \frac{\delta n_B(\mathbf{r}')}{\delta \psi(\mathbf{r})} \frac{\delta F^{(0)}}{\delta n_B(\mathbf{r}')} \right] d\mathbf{r}' \\ &= \frac{\mu_A(\mathbf{r}) - \mu_B(\mathbf{r})}{2},\end{aligned} \tag{B2}$$

where $F^{(0)}$ is the static part of the free energy, $F^{(0)} = F(\mathbf{v}=\mathbf{0})$, and $\mu_A \equiv \delta F^{(0)}/\delta n_A$ and $\mu_B \equiv \delta F^{(0)}/\delta n_B$ are the static chemical potentials of species A and B, respectively. Then using Gibbs-Duhm relation $s dT - dP + \Sigma_{i=A,B} n_i d\mu_i = 0$, where $s \equiv S/V$ is the entropy density, and also using the relation $n_A d\mu_A + n_B d\mu_B = n d\mu_n + \psi d\mu_\psi$, we have $s dT - dP + n d\mu_n + \psi d\mu_\psi = 0$ or $s\nabla T - \nabla P + n\nabla\mu_n + \psi\nabla\mu_\psi = \mathbf{0}$. Under the constant temperature the first term vanishes. Then using this we rewrite P in Eq. (34) to obtain

$$\rho \frac{d\mathbf{v}}{dt} = -\rho(\mathbf{v}\cdot\nabla)\mathbf{v} + \eta\nabla^2\mathbf{v} - n\nabla\mu_n - \psi\nabla\mu_\psi, \tag{B3}$$

where

$$\begin{aligned}\mu_n &\equiv \frac{\delta F^{(0)}}{\delta n} = \chi^{-1}(n - n_0), \\ \mu_\psi &\equiv \frac{\delta F^{(0)}}{\delta \psi} = \frac{\delta F}{\delta \psi} = -g\nabla^2\psi - \psi + \psi^3.\end{aligned} \tag{B4}$$

We must show that the free energy (29) does not increase. This is a necessary condition for phenomenological equations. Let us consider the time derivative of the free energy

$$\begin{aligned}\frac{dF}{dt} &= \int \left(\dot{\mathbf{v}} \frac{\delta F}{\delta \mathbf{v}} + \dot{n} \frac{\delta F}{\delta n} + \dot{\psi} \frac{\delta F}{\delta \psi} \right) d\mathbf{r} \\ &= \int \left[\dot{\mathbf{v}} \cdot \mu_v + \dot{n} \left(m \frac{v^2}{2} + \mu_n \right) + \dot{\psi}\mu_\psi \right] d\mathbf{r},\end{aligned} \tag{B5}$$

where

$$\boldsymbol{\mu}_v \equiv \frac{\delta F}{\delta \mathbf{v}} = \rho \mathbf{v}. \tag{B6}$$

By substituting equations for ψ, n, and $\mathbf{v}$, i.e., Eqs. (30)–(33) and (B3), into Eq. (B5) we have

$$\frac{dF}{dt} = \int \left\{ \mathbf{v} \cdot \left(-\rho \nabla \frac{v^2}{2} + \eta \nabla^2 \mathbf{v} - n \nabla \mu_n - \psi \nabla \mu_\psi \right) + \left(\frac{m v^2}{2} + \mu_n \right) [-\nabla \cdot (n \mathbf{v}) + L_n \nabla^2 \mu_n^*] + \mu_\psi [-\nabla \cdot \psi \mathbf{v} + L_\psi \nabla^2 \mu_\psi] \right\} d\mathbf{r}, \tag{B7}$$

where in the first term we used $\mathbf{v} \cdot [(\rho \mathbf{v} \cdot \nabla)\mathbf{v}] = (\rho \mathbf{v} \cdot \nabla) v^2/2$. By rearranging terms with the aid of the partial integration we have

$$\frac{dF}{dt} = \int \left(-\rho \mathbf{v} \cdot \nabla \frac{v^2}{2} - \frac{v^2}{2} \nabla \cdot \rho \mathbf{v} \right) d\mathbf{r} - \int (-\eta \mathbf{v} \cdot \nabla^2 \mathbf{v} + L_\psi |\nabla \mu_\psi|^2 + L_n |\nabla \mu_n'|^2) d\mathbf{r}. \tag{B8}$$

The first term is reduced to the surface integration $-\int \nabla \rho \mathbf{v} (v^2/2) d\mathbf{r}$ and vanishes. Finally, we find that the free energy does not increase:

$$\frac{dF}{dt} = -\int \left[-\eta \mathbf{v} \cdot \nabla^2 \mathbf{v} + L_\psi |\nabla \mu_\psi|^2 + L_n \left| \nabla \left(m \frac{v^2}{2} + \mu_n \right) \right|^2 \right] d\mathbf{r} \leqslant 0. \tag{B9}$$

We comment here on Eq. (B3). By rewriting Eq. (B9) with the use of kinetic equations (30)–(33) and (B3) we have

$$\frac{dF}{dt} = -\eta^{-1} \int \left(\rho \frac{d\mathbf{v}}{dt} + n \nabla \mu_n + \psi \nabla \mu_\psi \right) \nabla^{-2} \left(\rho \frac{d\mathbf{v}}{dt} + n \nabla \mu_n + \psi \nabla \mu_\psi \right) d\mathbf{r} - L_n^{-1} \int \left(\frac{dn}{dt} + \nabla \cdot n \mathbf{v} \right) \times \nabla^{-2} \left(\frac{dn}{dt} + \nabla \cdot n \mathbf{v} \right) d\mathbf{r} - L_\psi^{-1} \int \left(\frac{d\psi}{dt} + \nabla \cdot \psi \mathbf{v} \right) \times \nabla^{-2} \left(\frac{d\psi}{dt} + \nabla \cdot \psi \mathbf{v} \right) d\mathbf{r}. \tag{B10}$$

Here we have neglected the temperature term and nonlinear term of velocity field. In Eq. (B10) the second and the third term are the product of quantities that satisfy the conservation law. By this reason the long-range integration of these terms gives a finite contribution. But the first term is not of such a form. The first term on the right-hand side is written, using the Fourier coefficient, as

$$\int \eta^{-1} k^{-2} \left| \left(\rho \frac{d\mathbf{v}_\mathbf{k}}{dt} + n \nabla \mu_n + \psi \nabla \mu_\psi \right)_\mathbf{k} \right|^2 k^{d-1} dk = \int \eta |\mathbf{v}_\mathbf{k}|^2 k^{d+1} dk. \tag{B11}$$

Here $\mathbf{v}$ and each term in the large parentheses on the left-hand side are nonconserved quantities. Namely, μ is a nonlinear function of a conserved quantity and is a nonconserved quantity. The product of the conserved quantity is generally nonconserved. Then the time derivative of $\mathbf{v}$, which contains $\psi \nabla \mu_\psi$, is nonconserved. We may assume that the spatial correlation between two nonconserved quantity vanishes if two points are separated by a sufficiently long distance. Then from the central limit theorem, mean squares of these quantities take constant values at small wave numbers. For instance, $\lim_{k \to 0} \langle |\mathbf{v}_\mathbf{k}|^2 \rangle = \text{const} < \infty$. Therefore contributions from small values of $\mathbf{k}$ are $\int k^{d-3} dk$ on the left-hand side of Eq. (B11) and $\int k^{d+1} dk$ on the right-hand side. Therefore, in the limit $k \to 0$, we demand that

$$\rho \frac{d\mathbf{v}}{dt} + n \nabla \mu_n + \psi \nabla \mu_\psi \to 0 \quad \text{for } d \leqslant 2 \tag{B12}$$

and

$$\left| \rho \frac{d\mathbf{v}}{dt} + n \nabla \mu_n + \psi \nabla \mu_\psi \right| < \infty \quad \text{for } d > 2. \tag{B13}$$

Therefore, in two dimensions the inertial term $\rho d\mathbf{v}/dt$ cannot be neglected if the force term $n \nabla \mu_n + \psi \nabla \mu_\psi$ does not vanish at small wave numbers.

APPENDIX C: INCOMPRESSIBLE FLUID (LINEAR CASE)

In fluid the assumption of incompressibility is often used. This assumption can be used to eliminate the velocity field $\mathbf{v}$ and to make a closed equation for ψ. In order to make the fluid incompressible we assume that the change in the density due to the diffusion is very small: $L_n \to 0$. Since n is constant, $0 = \dot{n} = -n \nabla \cdot \mathbf{v} + L_n \nabla^2 \mu_n$ from Eqs. (30) and (32). In the limit $L_n \to 0$, we have $\nabla \cdot \mathbf{v} = 0$. But we cannot simply set $\nabla \cdot \mathbf{v} = 0$. This is because we must treat the transmission of the force in fluid. Thus we assume that $\nabla \cdot \mathbf{v}$ is very small compared to $\nabla^2 \mu_n$. Inserting ∇ into the linearized equation (36), we have

$$\rho \frac{d}{dt} \nabla \cdot \mathbf{v} = \eta \nabla^2 \nabla \cdot \mathbf{v} - n \nabla^2 \mu_n - \nabla \cdot (\psi \nabla \mu_\psi). \tag{C1}$$

Here the second term on the right-hand side is equivalent to $L_n^{-1} n^2 \nabla \cdot \mathbf{v}$ and is much larger than the left-hand side and the first term on the right-hand side. The left-hand side and the first term on the right-hand side are smaller than any other terms. Therefore, $-n \nabla^2 \mu_n - \nabla \cdot (\psi \nabla \mu_\psi) = 0$. To solve this equation for $\nabla \mu_n$ we multiply the equation by $\nabla \nabla^{-2}$, i.e., $-n \nabla \mu_n = \nabla \nabla^{-2} \nabla \cdot (\psi \nabla \mu_\psi)$. By substituting this into the linearized equation (36) we obtain

$$\rho\frac{d\mathbf{v}}{dt}=\eta\nabla^2\mathbf{v}-(\mathsf{I}-\nabla^{-2}\nabla:\nabla)\psi\nabla\mu_\psi$$
$$=\eta\nabla^2\mathbf{v}-\eta\int\nabla^2\mathsf{T}(\mathbf{r}-\mathbf{r}')\psi(\mathbf{r}')\nabla'\mu_\psi(\mathbf{r}')d\mathbf{r}'. \quad \text{(C2)}$$

Here T is the Oseen tensor

$$\mathsf{T}(\mathbf{r}-\mathbf{r}')\equiv\eta^{-1}\nabla^{-2}(\mathsf{I}-\nabla^{-2}\nabla:\nabla)\delta(\mathbf{r}-\mathbf{r}')$$
$$=(8\pi^3\eta)^{-1}\int k^{-2}(\mathsf{I}-\hat{\mathbf{k}}:\hat{\mathbf{k}})e^{i\mathbf{k}\cdot\mathbf{r}-\mathbf{r}'}d\mathbf{k}. \quad \text{(C3)}$$

where $\mathbf{k}$ and $\hat{\mathbf{k}}\equiv\mathbf{k}/k$ are the wave-number vector and the unit wave-number vector, respectively. For viscous fluid this is solved to give a well-known kinetic equation for ψ [30]. The inertial term can be neglected when the viscosity is large. By setting the left-hand side of Eq. (C2) equal to zero we have $\mathbf{v}=\int\mathsf{T}(\mathbf{r}-\mathbf{r}')\psi(\mathbf{r}')\nabla'\mu_\psi(\mathbf{r}')d\mathbf{r}'$. By substituting this into Eq. (31), we have

$$\frac{d\psi}{dt}=L_\psi\nabla^2\mu_\psi+\nabla\psi\int:\mathsf{T}(\mathbf{r}-\mathbf{r}'):\psi(\mathbf{r}')\nabla'\mu_\psi(\mathbf{r}')\,d\mathbf{r}'$$
$$=L_\psi\nabla^2\mu_\psi-\nabla\psi\int:\mathsf{T}(\mathbf{r}-\mathbf{r}'):[\nabla'\psi(\mathbf{r}')]\mu_\psi(\mathbf{r}')\,d\mathbf{r}'. \quad \text{(C4)}$$

Here we have used $\psi\nabla\mu=\nabla(\mu\psi)-(\nabla\psi)\mu$ and $\mathsf{T}\nabla=0$ to transform the first equality into the last one.

[1] J. D. Gunton, M. San Miguel, and P. S. Sani, in *Phase Transitions and Critical Phenomena*, edited by C. Domb and J. L. Lebowitz (Academic, London, 1983), Vol. 8.
[2] H. Furukawa, Adv. Phys. **34**, 703 (1984).
[3] K. Binder, in *Material Sciences and Technology*, edited by R. W. Cohen, P. Haasen, and E. J. Kramer (VCH, Weinheim, 1991), Vol. 5, p. 405.
[4] G. F. Mazenko, Phys. Rev. B. **43**, 8204 (1991).
[5] T. Hasimoto, in *Materials Science and Technology*, edited by R. W. Cohen, P. Haasen, and E. J. Kramer (VCH, Weinheim, 1993), Vol. 12, p. 252.
[6] A. Shinozaki and Y. Oono, Phys. Rev. E **48**, 2622 (1993).
[7] A. J. Bray, Adv. Phys. **43**, 357 (1994).
[8] H. Furukawa, Phys. Rev. A **31**, 1103 (1985); Physica A **204**, 237 (1994).
[9] O. T. Valls and G. F. Mazenko, Phys. Rev. B **38**, 11 643 (1988).
[10] J. E. Farrel and O. T. Valls, Phys. Rev. B **40**, 7027 (1989); **42**, 2353 (1990).
[11] Y. Wu, F. J. Alexander, T. Lookman, and S. Chen, Phys. Rev. Lett. **74**, 3852 (1995).
[12] W. J. Ma, A. Maritan, J. Banavar, and J. Koplik, Phys. Rev. A **45**, 5347 (1992).
[13] E. Valasco and S. Toxvaerd, Phys. Rev. Lett. **71**, 388 (1993).
[14] P. Ossadnik, M. F. Gryre, H. E. Stanley, and S. Glotzer, Phys. Rev. Lett. **72**, 2498 (1994).
[15] G. Leptoukh, B. Strickland, and Roland, Phys. Rev. Lett. **74**, 3636 (1995).
[16] F. F. Abraham, S. W. Koch, and R. C. Desai, Phys. Rev. Lett. **49**, 923 (1982).
[17] F. I. Alexander, S. Chen, and D. W. Grunau, Phys. Rev. B **48**, 634 (1993).
[18] S. Bastea and J. L. Lebowitz, Phys. Rev. E **52**, 3821 (1995).
[19] W. R. Osborn, E. Orlandini, M. F. Swift, J. M. Yeomans, and J. R. Banavar, Phys. Rev. Lett. **75**, 4031 (1995).
[20] P. B. S. Kumar and M. Rao, Phys. Rev. Lett. **77**, 1067 (1996).
[21] A. Onuki, Phys. Rev. A **34**, 3528 (1986).
[22] E. D. Siggia, Phys. Rev. A **20**, 595 (1979); N. C. Wang and C. M. Knobler, J. Chem. Phys. **69**, 725 (1978); Phys. Rev. A **24**, 3205 (1981); Y. C. Chou and W. I. Goldburg, *ibid*. **20**, 2105 (1979); **23**, 858 (1981); N. Kuwahara, M. Tachikawa, K. Hamano, and Y. Kenmochi, *ibid*. **25**, 3449 (1982); D. Beysens, P. Guenoun, and F. Perrot, in *Dynamics of Ordering Processes in Condensed Matter*, edited by S. Komura and H. Furukawa (Plenum, New York, 1988), p. 373.
[23] P. Berg, Y. Pomeau, and Ch. Vidal, *Order in Chaos* (Hermann, Paris, 1984); D. J. Evans and G. P. Morris, *Statistical Mechanics of Nonequilibrium Liquids* (Academic, San Diego, 1990).
[24] K. Binder and D. Stauffer, Phys. Rev. Lett. **33**, 1006 (1974).
[25] See, for example, *Computer Simulations Using Particles*, edited by P. W. Hockny and J. W. Eastwood (McGraw-Hill, New York, 1981).
[26] Y. G. Sinai, Russ. Math. Surveys **25**, 137 (1970).
[27] Y. Oono and S. Puri, Phys. Rev. Lett. **58**, 836 (1987); Phys. Rev. A **38**, 434 (1988); S. Puri and Y. Oono, *ibid*. **38**, 1542 (1988).
[28] K. Kawasaki, Ann. Phys. (N.Y.) **61**, 1 (1970); B. I. Halperin, P. C. Hohenberg, and E. D. Siggia, Phys. Rev. Lett. **32**, 1289 (1974); see also [10].
[29] J. W. Cahn, Trans. AIME **242**, 166 (1967).
[30] K. Kawasaki, in *Synergetics*, edited by H. Haken (Teubner, Stuttgart, 1973), p. 35; K. Kawasaki and T. Ohta, Physica A **118**, 175 (1983).
[31] A. Onuki, Prog. Theor. Phys. **74**, 1155 (1985); H. Hayakawa and T. Koga, J. Phys. Soc. Jpn. **59**, 3542 (1990); A. J. Bray and A. D. Rutenberg, Phys. Rev. E **49**, R27 (1994).